Z. Phys. A – Atomic Nuclei 333, 45–56 (1989)

Zeitschrift für Physik A
Atomic Nuclei

Analysis of Excitation Functions from Light Ion Induced Reactions in the EXCLUSIVE INDEX Model*

J. Ernst, W. Friedland, and H. Stockhorst**
Institut für Strahlen- und Kernphysik der Universität Bonn,
Federal Republic of Germany

Received September 26, 1987; revised version December 20, 1988

The previously introduced EXCLUSIVE INDEX model allows to predict the population of 6 residual nuclei including the primary compound nucleus through two stages of the preequilibrium phase. The present version is limited to maximum two-nucleon emission. The preequilibrium ejectiles may reduce the brought-in rotational energy by a model of maximum angular momentum decoupling. Subsequent evaporation of protons, neutrons and α-particles is treated in the frame of the Weisskopf-Ewing and s-wave approximation considering pairing effects only in compound nucleus state densities. The sensitivity of essential preequilibrium parameters on the shape of calculated excitation functions is tested. The model predictions well compare to excitation functions from p, d, ^{3}He and ^{4}He induced reactions including the large set from the reaction ^{93}Nb(^{4}He, $xn\,yp$) up to 170 MeV bombarding energy. The general importance of two-nucleon preequilibrium emission is accentuated in several examples. The deduced preequilibrium parameters corroborate the results from the INDEX model analysis of nucleon spectra.

PACS: 24.60.Dr; 24.60.Gv; 25.40.–h; 25.45.–z; 25.55.–e; 25.70.Gh

1. Introduction

In a recently published paper [1] we have developed a detailed precompound model of *ind*ependently interacting *ex*citons (INDEX model) resuming the basic ideas of a previous investigation [2]. Here, we may only recall the basic statistics of the INDEX model [3, 4]; the n excitons of any stage, i.e. p particles and h holes, which are not emitted undergo two-body collisions and create further particle-hole pairs independently from each other. Thus the energy of an exciton is redistributed on three excitons of the following stage. The total number of excitons increases from stage μ to stage $\mu+1$ by a factor of three neglecting particle emission ($n_{(\mu+1)}=3n_{(\mu)}$). The proliferation of particles and holes is given by the recurrence relations $p_{(\mu+1)}=2p_{(\mu)}+h_{(\mu)}$ and $h_{(\mu+1)}=p_{(\mu)}+2h_{(\mu)}$. At the one hand this preequilibrium model is capable to predict inclusive proton and neutron spectra (INCLUSIVE INDEX model) comprising multi-nucleon preequilibrium emission up to any order of practical importance. With some restricting assumptions, on the other hand, a second version of the model allows to determine exclusive nucleon spectra being needed, e.g. for calculating residual nucleus excitation functions (EXCLUSIVE INDEX model).

In a subsequent investigation [5] we have compared and inter-compared both versions of the INDEX model to inclusive nucleon spectra from p-, α- and stopped π^--induced reactions up to 170 MeV initial energy. The theme of the present study is a rigorous test of the predictive power of the EXCLUSIVE INDEX model regarding excitation functions from light ion induced reactions.

Residual nucleus excitation functions naturally cover a wide range of bombarding energies. Hence, they complement the knowledge gained from the study of inclusive particle spectra and supply valuable information on the division of the total reaction cross section into specific exit channels.

* Dedicated to Professor Theo Mayer-Kuckuk on the occasion of his 60th birthday

** Present address: Gesellschaft für Strahlen- und Umweltforschung mbH München, Ingolstädter Landstrasse 1, D-8042 Neuherberg, Federal Republic of Germany

These are characterized by the number of protons and neutrons which have been emitted from the composite system of target and projectile. In [1, 4] we have outlined the new and powerful method for computing the exclusive reaction probability to populate an arbitrary energy bin of a certain residual nucleus. The actual code [6] is capable of computing excitation functions including the preequilibrium emission (PE) of up to two nucleons in two stages. The formalism comprises 15 principal paths to attain nuclear equilibrium. One leads to the compound nucleus of the initial projectile-target system while the other 14 lead to the 5 residual nuclei which can be reached by PE emission of one or two nucleons. E.g., the residual nucleus with $\Delta Z=1$ and $\Delta N=1$ can be reached via four different paths: Proton-neutron emission from the first and second PE stage and two cascades with a proton (neutron) being emitted from the first PE stage followed by a neutron (proton) from the second one.

In Sect. 2 we recall the important input parameters of the EXCLUSIVE INDEX model including the option of angular momentum decoupling in preequilibrium emission which gets important for heavier projectiles. In Sect. 3 we sketch the formalism underlying the subsequent compound nucleus (CN) decay chain calculations. Here, one may account for effects of the brought-in rotational energy in the frame of the *s*-wave approximation [7]. The latter is a special case of a more generalized approximation treating average angular momentum decoupling in CN evaporation which we introduce in the appendix. The comparison of EXCLUSIVE INDEX model predictions with excitation functions from light ion induced reactions is the main theme of Sect. 4. The conclusions drawn from the present investigation are summarized in the last section.

2. Important Parameters Determining Preequilibrium Emission

2.1. The Fermi Energy and Related Parameters

In the INDEX model particles and holes occupy available s.p. states of a Fermi gas. At the Fermi level, the s.p. state density g is related to the Fermi energy E_F according to $E_F=1.5\ A/g$ holding for nuclei with $Z\approx N$. Our preferred choice is $g=A/13.3\ \mathrm{MeV}^{-1}$ corresponding to a maximum hole depth of $E_F=20$ MeV. For simplicity we assume that g is constant. These Fermi gas parameters have to be used in a consistent fashion. They determine the nuclear density and influence the velocity of particles inside the nuclear medium as well as the amount of Pauli blocking of available final states. Hence, they strongly influence the continuum escape probability of an exciton particle. The overall strength of calculated PE emission spectra and excitation functions can be adjusted by the empirical "mean-free-path" multiplier k_{MFP} which is usually $\geqq 1$ and reduces the rate of nucleon-nucleon collisions in nuclear matter.

2.2. The Set of Initial Exciton Numbers

The shape of spectra and excitation functions are very sensitive to the initial exciton number n_0 which is the sum of p particles and h holes. With the indices π indicating protons and ν neutrons the total set of initial exciton numbers is written $n_0(p_\nu, p_\pi)$ with $h=n_0-p_\nu-p_\pi$. These numbers need not to be integers so that a continuous averaging between succeeding integers is possible. Our standard choice, $n_0=A_{\mathrm{Proj.}}+2$, is in accordance with the idea that the projectile dissolves into its constituent nucleons following the first $p-h$ excitation of the target nucleus. The well known free nucleon-nucleon scattering cross section relation [8], namely σ_{pn}: σ_{pp}: $\sigma_{nn}=3:1:1$ is assumed to hold throughout the nuclear equilibration. It enters into the calculation of the particle numbers p_ν and p_π of the first and second PE stage thereby determining the relative strength of proton and neutron exciton distributions [1, 4]. Since we do not specify the charge of holes a first stage hole creates second stage particles of type π or ν with equal probability. The neglect of the finite hole depth E_F in the evaluation of exciton distributions can be compensated by an appropriate reduction of the initial hole number h, and hence of n_0, as well as by increasing the value of k_{MFP} (cf. Sect. 2.1).

2.3. Angular Momentum Effects

For heavier projectiles, typically with $Z\geqq 2$, angular momentum effects in PE processes have to be considered. In [5] we have introduced a simple model in which part (L_{out}) of the brought-in angular momentum L_{in} is removed from the system by one or two fast PE particles assuming maximum angular momentum decoupling [9]. It is assumed that the remaining rotational energy $E_{rot}(L_{in}-L_{out}, Z', N', U')$ is not available for PE emission and subsequent CN evaporations. Hence, this rotational energy may be subtracted from the excitation U' of the intermediate nuclei following PE emission. This option is used together with the *s*-wave approximation for CN emission of particles (see below).

3. Important Parameters Determining Equilibrium Emission

For the evaporation part of the code INDEX [6] the code OVERLAID ALICE [10] is employed with the few modifications as mentioned below.

3.1. *Standard Options for Target and Projectile Parameters*

The total reaction cross sections for ^{3}He and ^{4}He projectiles were calculated from the the parabolic barrier approximation [11] while for protons and deuterons the inbuilt optical model subroutines were used (for details see [10]). The latter also provided the inverse cross sections for neutrons, protons and ^{4}He particles in the exit channels. Since the inclusion of neither d, t and ^{3}He evaporation particles nor of fission had noticable effects on calculated excitation functions for nuclei $89 \leqq A \leqq 209$ these optional decay modes [3, 6, 10] were neglected throughout. All binding energies were deduced from inbuilt experimental mass tables [12, 13].

3.2. *Level Density Options*

Effective residual nucleus level densities at total excitation energy U' are calculated by

$$\rho_{\text{eff}}(U') = (U^* + \Delta)^r \exp\{2[a(U^* + \Delta)]^{1/2}\} \tag{1}$$

A 'soft pairing' correction [14]

$$\Delta = 12 n_u / A^{1/2} \tag{2}$$

is usually employed where n_u is the number of unpaired protons and neutrons in the nucleus. The positive pairing correction Δ avoids an effective change of thresholds which occurs in the more common form. There Δ gets negative for even and odd nuclei and is zero for doubly-odd ones. The equivalence $U' = U^*$ together with an exponent $r = -5/4$ is valid for the Weisskopf-Ewing approximation [15] while $r = -2$ holds for spin-dependent level densities [14]. For calculating effective excitation energies U^* the remaining rotational energy has to be subtracted from the total excitation energy U'. For the sake of a quite general formulation we write

$$U^* = U' - E_{\text{rot}}(J'_{\text{eff}}(x, \varepsilon, J)) \tag{3}$$

where $J'_{\text{eff}}(x, \varepsilon, J)$ has the meaning of a suitably chosen average total spin of the residual nucleus being formed by the emission of particle x with kinetic energy ε_x from the preceding compound nucleus of total spin J. As outlined in the Appendix this ansatz allows to retain the practical features of the Weisskopf-Ewing approximation, i.e. the use of inverse cross sections instead of summing over angular momentum and channel spin dependent transmission coefficients. This latter Hauser-Feshbach approach [16] is rather prohibitive for computing long evaporation cascades. In the present paper we use the most simple approach, the s-wave approximation [7]:

$$E_{\text{rot}}(J'_{\text{eff}}(x, \varepsilon, J)) = E_{\text{rot}}(J) = J(J+1)\,\hbar^2/2\theta \tag{4}$$

where θ is the moment of inertia of the emitting CN. N.B., the assumption $J'_{\text{eff}} = J$ only means that *on average* the residual nucleus keeps the spin J of the parent CN. Thus, the usual name "s-wave approximation" is somewhat misleading (see Appendix). It follows that the original rotational energy of the primary compound nucleus, or the left-over rotational energy in the intermediary nuclei following PE emission is frozen-in and can be subtracted from the available excitation energy. Then, one may easily integrate over the incoming partial waves contributing to different bins of the effective excitation energy – a procedure considerably simplifying the calculations of subsequent CN cascades [10].

3.3. *Parameter Choice*

Since many parameters enter into the INDEX model calculations a very large number of different input options can be selected. In order to allow for a reasonable comparison of theory and experiment, however, we keep fixed the relevant parameters as much as possible. Regarding the projectile and target dependence of evaporation cascades two exceptions from this 'rule' are made:

a) While for proton and deuteron induced reactions the Weisskopf-Ewing approximation is applied, the s-wave approximation is used for ^{3}He and ^{4}He induced reactions together with angular momentum decoupling in the PE emission of nucleons (see above). The rotational energies were calculated from the moments of inertia due to the liquid drop model [17]. Figure 7b illustrates the differences resulting from both approaches.

b) To keep the code managable the level density parameter a is taken to be the same for all residual nuclei which is a rather drastic assumption. By varying this global parameter the shape of evaporation spectra, and even more important the relative flux into proton and neutron channels can be adjusted.

For target nuclei $A \leqq 93$ we took the standard value $a = A/8$ while for nuclei $A \geqq 181$ we found $a = A/13$ to be a better choice.

4. Comparison of Calculated and Measured Excitation Functions

4.1. General Dependence on Preequilibrium Model Parameters

The general sensitivity of the shape and height of excitation functions on the parameters n_0, E_F and k_{MFP} is demonstrated in Fig. 1. The 5 excitation functions of the reaction ^{93}Nb(^{4}He, $xn\,yp$) with $y = 0$, 1, 2, 4 and 6 and $x + y = 3$, 4, 7, 11 and 15, respectively, give examples for small, medium and large numbers of removed protons and neutrons. In the experiment [18] the corresponding residual nuclei could be well separated from neighbouring feeding isobars thus representing a valuable sample for theoretical comparisons (cf. Figs. 8–12 in Subsect. 4.5). The figure complements Fig. 5 in [1] where the division of the total reaction flux into CN formation, and one- and two-nucleon emission was studied for different values of n_0, k_{MFP} and E_F. The purely theoretical predictions

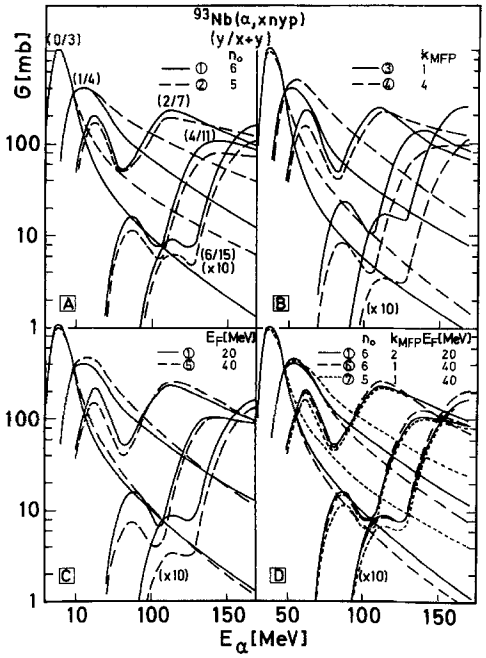

Fig. 1A–D. Calculated excitation functions of the reaction ^{93}Nb(^{4}He, $xn\,yp$) with $(y/x+y)$ as indicated in the figure. **A**, **B** and **C** show the effect of varying the parameters n_0, k_{MFP} and E_F, respectively, while keeping fixed the other quantities of the standard version ($n_0 = 6$, $E_F = 20$ MeV, $k_{MFP} = 2$). **D** compares different parameter sets of Table 1 which fit the data about equally well

Table 1. Different sets of input parameters used in the analysis of the ^{181}Ta, ^{93}Nb(^{4}He, $xn\,yp$) reaction

#	$n_0(p_\nu, p_\pi)$	k_{MFP}	E_F(MeV)
(1)	6(2.5, 2.5)	2	20
(2)	5(2.5, 2.5)	2	20
(3)	6(2.5, 2.5)	1	20
(4)	6(2.5, 2.5)	4	20
(5)	6(2.5, 2.5)	2	40
(6)	6(2.5, 2.5)	1	40
(7)	5(2.5, 2.5)	1	40

in Fig. 1 base on the sets of input parameters listed in Table 1.

Figure 1A proves that a variation of n_0 mostly affects the shape of excitation functions with zero or one emitted proton. The variation of the parameter k_{MFP} mainly influences the height of the predicted yields. While in Fig. 1B the assumption of a long mean free path ($k_{MFP} = 4$) increases the yield for residual nuclei with $\Delta A \leqq 7$, at the same time the reaction flux into nuclei with $\Delta A > 7$ is strongly reduced. The increase of E_F in Fig. 1C has similar but less pronounced effects. At bombarding energies below 140 MeV the PE emission is somewhat stronger for $E_F = 40$ MeV than for $E_F = 20$ MeV so that generally less flux is available for multi-nucleon evaporation. Figure 1D shows the sets which – depending on ΔA – best describe the measured excitation functions. As can be learned from comparing set (1) and (6) an increase of the finite hole depth E_F by a factor of 2 is practically compensated by a corresponding decrease of k_{MFP}. The same is true for the calculations (7) in Fig. 1D and (2) in Fig. 1A. This fact corroborates our conclusions on the parameter dependence of the particle escape probability in Sect. 5.1. of [1]. On the whole, it is found that the input parameter sets (1), (2), (6) and (7) are about equivalent for $\Delta A \geqq 7$ while the smaller value of $n_0 = 5$ in set (2) and (7) leads to higher tails of the (^{4}He, xn) and (^{4}He, $p\,xn$) excitation functions.

4.2. Comparison with Proton Induced Reactions

Figures 2–4 show a comparison of INDEX model calculations with excitation functions from the (p, xn) and $(p, p'xn)$ reactions on ^{89}Y [19] and ^{209}Bi [20] (cf. [5] for the corresponding analysis of p-spectra at $E_p = 62$ MeV). The use of the 'standard' values for $E_F = 20$ MeV, $k_{MFP} = 4$ and $n_0 = 2.5$ give the best agreement with the experimental data. Smaller values of k_{MFP} generally result in higher maxima in the (p, xn) and $(p, p'xn)$ excitation functions together with lower yields in the corresponding tails. For ^{89}Y we use a

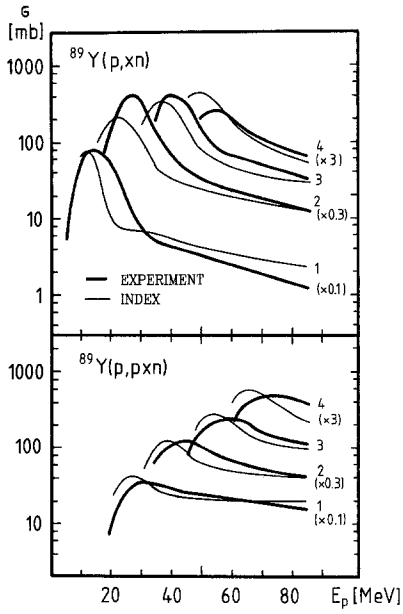

Fig. 2. $^{89}Y(p, xn)$ and $^{89}Y(p, p'xn)$ excitation functions in comparison with INDEX model predictions. Thick curves: experiments [19]; thin curves: calculations with $n_0=2.5(0.67, 1.33)$, $k_{MFP}=4$ and $E_F=20$ MeV

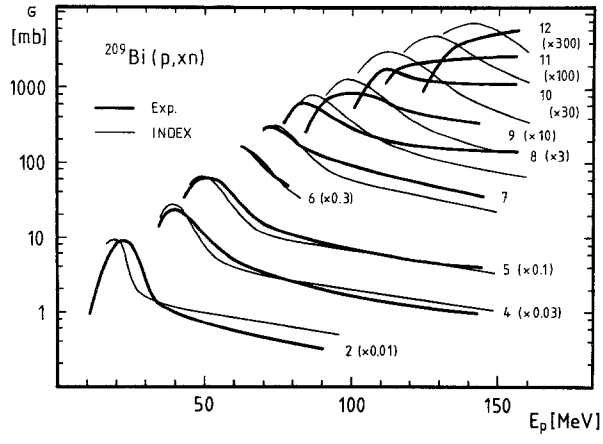

Fig. 3. $^{209}Bi(p, xn)$ excitation function in comparison with INDEX model predictions. Thick curves: experiments [20]; thin curves: calculations with $n_0=2.5(0.75, 1.25)$, $k_{MFP}=4$ and $E_F=20$ MeV. Each excitation function is labelled by the neutron multiplicity x

neutron to proton ratio of $p_\nu/p_\pi=0.67/1.33$ (Fig. 2). By this choice we use the same input parameters E_F and k_{MFP} as Gadioli et al. [21] for the EXCITON model analysis of the same data set $^{89}Y+p$. Our choice of $k_{MFP}=4$ and $n_0=2.5$ instead of $n_0=3$ in [21] practically compensates for effects of the limited hole depth E_F which could not be included in the computation of particle densities in the EXCLUSIVE INDEX model but is accounted for in the EXCITON model calculations. For $^{209}Bi(p_\nu/p_\pi=0.75/1.25)$ we

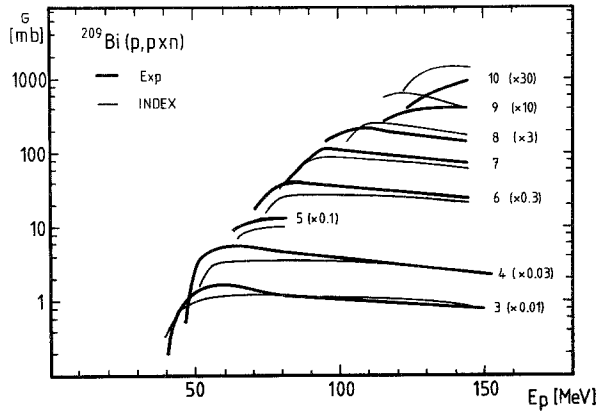

Fig. 4. $^{209}Bi(p, p'xn)$ excitation function in comparison with INDEX model predictions. The data are taken from [20]. The notation and model parameters are the same as in Fig. 3

notice typical deviations for proton energies above 120 MeV and $x>7$ (Figs. 3, 4). After the steep rise at the reaction threshold, the experimental yields are practically constant or are even slowly increasing to higher energies. This feature means a stronger vanishing of the thermalization in the primary compound system than the EXCLUSIVE INDEX model predicts. It demonstrates that the present limitation of our approach to two contributing PE stages gets a rough approximation in nucleon induced reactions above 120 MeV.

4.3. *Comparison with d-Induced Reactions*

Several d-induced excitation functions have been reported up to 86 MeV bombarding energy [9, 22, 23, 24]. For a comparison of data with the INDEX model we selected the reaction on ^{181}Ta which had been measured by Bisplinghoff et al. [23] from 10 to 80 MeV (Fig. 5). The used input parameters $n_0=4(1.5, 1.5)$ and $k_{MFP}=4$ with $E_F=20$ MeV give the best agreement with the data. The somewhat earlier rise of the calculated excitation functions can be ascribed to the use of the Weisskopf-Ewing approach which does not account for angular momentum effects. It gets the better approximation the more particle are emitted since in real nuclei the initial rotational energy is not available for few nucleon emission but is gradually regained in multi-particle cascades. It is interesting to note that the predictions for the (d, p) reaction, which is strongly enhanced by the stripping reaction, are off from the experimental yields by a factor of 20 to 30 while the $(d, 2p)$ and $(d, p4n)$ calculations are in excellent agreement with the data. The latter prove the importance of PE emission of one or even two nucleons. In previous Monte Carlo type equilibrium calculations with full angular momentum

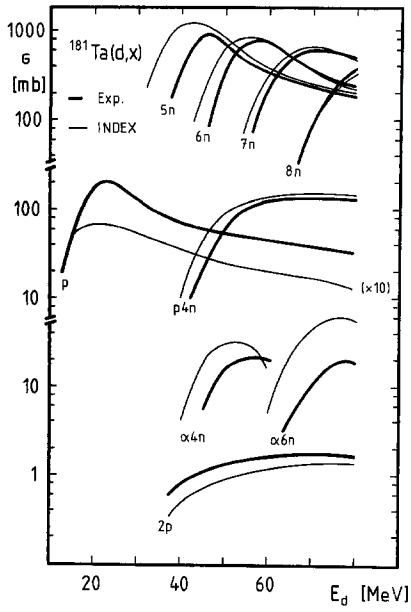

Fig. 5. ^{181}Ta(d, X) excitation function in comparison with INDEX model predictions. Thick curves: Experimental data [23]; thin curves: INDEX model with $n_0=4(1.5, 1.5)$, $k_{MFP}=4$ and $E_F=20$ MeV. The excitation functions are labelled by the emitted particles X

coupling [23] practically no 'events' were gained for the (d, p) and (d, $2p$) reactions, and the computed yields for the (d, $p4n$) reaction were off the experiment by one to three orders of magnitude.

4.4. *Comparison with ^{3}He-induced Reactions*

The projectile ^{3}He is loosely bound like the deuteron, and is known for strong stripping processes and elastic and non-elastic breakup reactions [25]. Nevertheless, a comparison of experimental yields with calculations comprising PE and CN processes will show to which extend the effect of these truly direct reactions is taken care of in the present ansatz. As an example we analyze the extensive experimental data set on ^{197}Au by Bousshid et al. [26] which cover the energy range from 15 to 135 MeV for alltogether 15 excitation functions including many with $\Delta Z=1$ and 2 (Fig. 6A, B, C). Other PE analyses of ^{3}He induced reactions are reported in [9, 27]. For our calculations we use the 'standard' input $n_0=5(1.6, 2.4)$, $k_{MFP}=2$ and $E_F=20$ MeV. The shapes of the (^{3}He, xn) and (^{3}He, $p\,xn$) excitation functions are quite well reproduced (Fig. 6A, B). The use of the s-wave approximation well accounts for the rise of subsequent (^{3}He, xn) excitation functions. However, the experimental yields are generally much smaller than predicted (cf. the scaling factor of 0.6 in Fig. 6A). Contrasting the calculations, for $x=10$ the typical experimental evaporation

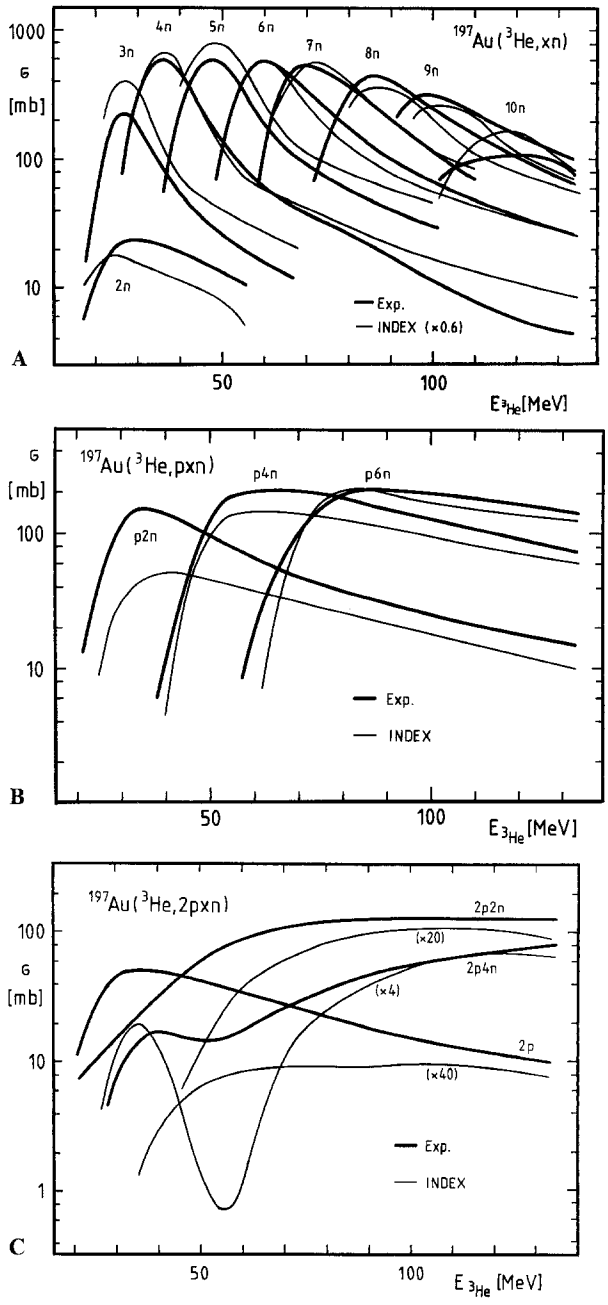

Fig. 6A–C. Excitation functions from ^{197}Au+^{3}He [25] (thick curves) in comparison with INDEX model predictions (thin curves) with the parameters $n_0=5(1.6, 2.4)$, $k_{MFP}=2$ and $E_F=20$ MeV. **A**, **B** and **C** present the ^{197}Au(^{3}He, xn), (^{3}He, $p\,xn$) and (^{3}He, $2p\,xn$) reactions, respectively

maximum vanishes proving that beyond 100 MeV at least the first particle out is due to a direct or PE process. The over-prediction for (^{3}He, xn) yields corresponds to an under-prediction of (^{3}He, $p\,xn$) processes that is lessened with increasing neutron numbers.

Quite strikingly, the flux into the (^{3}He, $2pxn$) channels is nearly as strong as that into (^{3}He, pxn)

(Fig. 6C). This feature is either tpyical for a strong (^{3}He, ^{4}He) pickup reaction (cf. $2p\,2n$ curve) or for a non-elastic breakup of ^{3}He into 2 spectator protons and a stripped off projectile-neutron being bound in ^{197}Au, or inducing a subsequent reaction [25] (cf. $2p$, $2p\,2n$ and $2p\,4n$ curves). Apparently, the INDEX model fails to reproduce these very direct processes up to a factor of 40. However, the mismatch decreases with increasing neutron number down to a factor of 4 regarding the $2p\,4n$ excitation function. The fact that the code does not account for PE ^{4}He emission explains the deep valley between the calculated (^{3}He, ^{4}He $2n$) evaporation maximum and the subsequent rise to the (^{3}He, $2p\,4n$) process.

4.5. Comparison with ^{4}He-Induced Reactions

For the study of PE effects besides nucleons ^{4}He is the ideal projectile since it is tightly bound and thus less amenable to stripping and pickup reactions. Here, we refer to previously published measurements on the reactions ^{93}Nb, ^{181}Ta(^{4}He, $yp\,xn$) up to 170 MeV [18]. The reaction on ^{93}Nb was also the theme of a parallel experimental as well as theoretical investigation by Gadioli et al. [28] comprising part of the Bonn data so that the INDEX model results can be compared with the predictions of the EXCITON model for α-induced reactions (see Sect. 5). The following INDEX model results for both targets are based on the parameter sets (1), (2), (4) and (7) of Table 1.

At first, in Fig. 7, the results for the ^{181}Ta + ^{4}He reaction are presented. For a better display we restrict the data in Fig. 7A to an even number of nucleons emitted from ^{185}Re*. Generally, set (1) better reproduces height and shape of the excitation functions while set (2) is merely of advantage for the case of (^{4}He, $2n$). A larger value of $a = A/8$ instead of the used one $a = A/13$ (see above) would result in a better fit of the maxima of the (^{4}He, ^{4}He'$(y-2)$ $p(x-2)$ n) excitation functions. Then however, other features of the theoretical prediction like the rise of the (^{4}He, xn) curves would deteriorate.

Figure 7B shows (for odd numbers of emitted nucleons) the improvement gained in using the s-wave approximation instead of the Weisskopf-Ewing description (dashed curves). Especially, at the higher energies the neglect of angular momentum effects leads to a much too early rise of the excitation functions. Switching off the 'soft pairing' option (cf. Chap. 3.2) does not produce a big difference to the standard WE calculation. However, such pairing effects have been found to be important when crossing closed shells by multi-nucleon emissions [9].

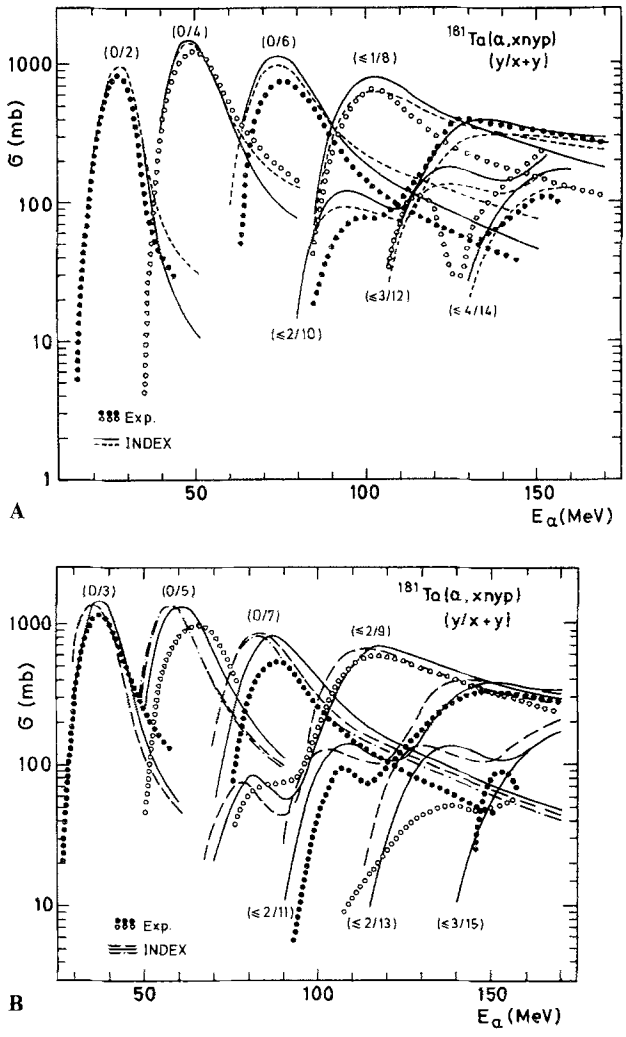

Fig. 7. A ^{181}Ta(^{4}He, $xn\,yp$) excitation functions in comparison with INDEX model predictions for even $x+y$ (labels $(y/x+y)$). Open and full circles represent the experimental data [18]. All INDEX model calculations use $k_{MFP}=2$ and $E_F=20$ MeV. Thin solid lines: standard option for $n_0=6(2.5, 2.5)$; thin dashed lines: standard option for $n_0=5(2.5, 2.5)$; **B** Data for odd $x+y$. Dashed lines: WE option with $n_0=6(2.5, 2.5)$; dashed-dotted lines: same parameters except pairing energy correction $\Delta=0$

For the ^{93}Nb(^{4}He, $yp\,xn$) reaction the standard option $a = A/8$ worked out quite sufficiently. As for other projectiles, excitation functions for $y \leqq 2$ and $x \leqq 4$ are most sensitive to the choice of the PE options (Figs. 8, 9). Since many residual activities could be followed over more than 100 MeV their typical PE tails provide a stringent test on the model parameters. We note that neither $n_0=5$ nor $n_0=6$ exactly reproduce the measurements. Typically, the sets (2) or (7) with $n_0=5$ best describe the (^{4}He, n), (^{4}He, $2n$) and (^{4}He, $2p$) reactions while for 3, 4 and more removed nucleons set (1) with $n_0=6$ gets more and more advantageous. Using a mean-free-path multiplier of $k_{MFP}=4$ in set (4) does not considerably improve

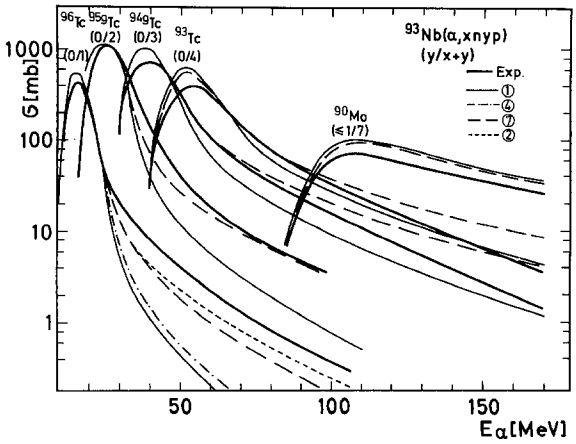

Fig. 8. ^{93}Nb(^{4}He, $xn\,yp$) excitation function in comparison with INDEX model predictions. The curves are labelled by their particle multiplicities ($y/x+y$). Thick curves: experimental data [18]; thin curves: INDEX model predictions where the encircled numbers denote the parameter sets listed in Table 1

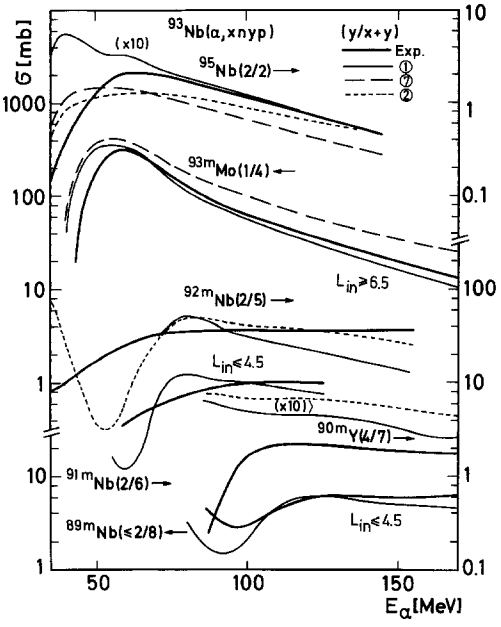

Fig. 9. ^{93}Nb(^{4}He, $xn\,yp$) excitation function in comparison with INDEX model predictions. Same notation as in Fig. 8. The employed cut-off angular momenta l_{co} are indicated for the case of low ($L_{in} \leqq l_{co}$) and high spin ($L_{in} \geqq l_{co}$) isomeres (see text)

the agreement. One explanation for this ambiguity is that for the emission of up to two protons or neutrons, the contribution of stripping reactions is not negligible, especially in the high energy tails [29], so that a smaller inital exciton number is better reproducing few nucleon emission. The relatively strong population of ^{95}Nb by the (^{4}He, $2p$) reaction is well reproduced by the curves with $n_0 = 5$ while that shown for $n_0 = 6$ is an order of magnitude off. This reaction

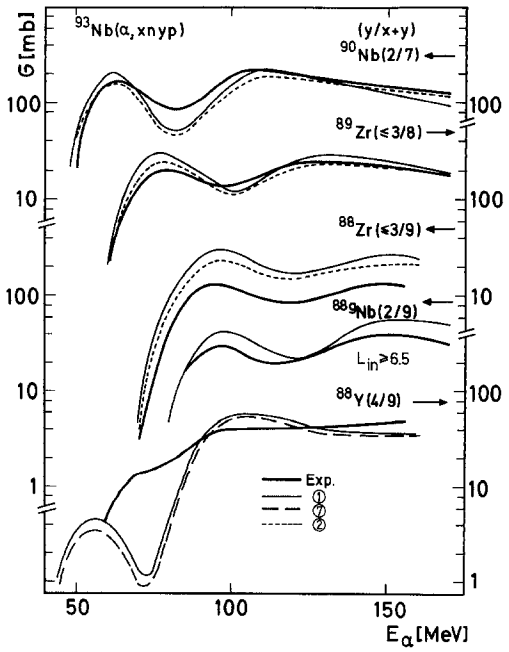

Fig. 10. ^{93}Nb(^{4}He, $xn\,yp$) excitation function in comparison with INDEX model predictions. Same notation as in Figs. 8 and 9

clearly demonstrates the importance of PE codes like the present one which allow for the emission of two PE nucleons. Calculations accounting only for one PE proton out and subsequent CN evaporation of a second one do miss the measured yields by orders of magnitude. The experimental yield for ^{90}Mo contains that for the neighbouring isobar ^{90}Tc which is indicated in Fig. 8 by the notation $(y/x+y)=(\leqq 1/7)$. The corresponding precdictions for ^{90}Tc were added to those of ^{90}Mo but were found to be rather weak. Here, the calculations (1) and (7) fit about equally well.

In Figs. 9–11 some curves correspond to isomer production yields. Fortunately, the s-wave approximation allows a rough theoretical estimate of isomeric yields: introducing a smooth cut-off angular momentum l_{co} the contribution to low spin isomeres is gained by multiplying each partial wave with angular momentum L_{in} by the factor $1/[1+\exp(L_{in}-l_{co})]$ while that for high spin isomers is obtained by the weight $(1-1/[1+\exp(L_{in}-l_{co})]\}$ [3, 4, 6]. This procedure holds for evaporation cascades from the primary compound nucleus. If PE emission precedes CN decay, the quantity L_{in} has to be substituted by the remaining angular momentum $L_{rem}(L_{in})$. The yield curve for ^{93m}Mo($I=21/2$) is excellently reproduced by the calculation using set (1) with a cut-off angular momentum $l_{co}=6.5$ while set (7) shows a too high PE tail as for ^{93,94}Tc. For the residual nuclei ^{90m}Y and ^{92,91m}Nb the calculations only give the right order of magnitude, which is to be expected since

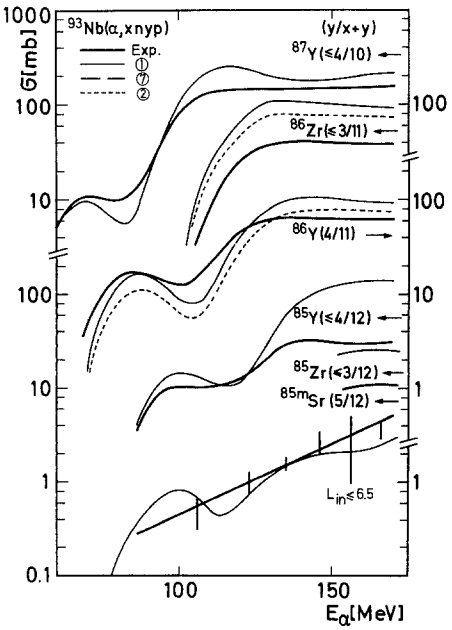

Fig. 11. ^{93}Nb(^{4}He, $xn\,yp$) excitation function in comparison with INDEX model predictions. Same notation as in Figs. 8 and 9

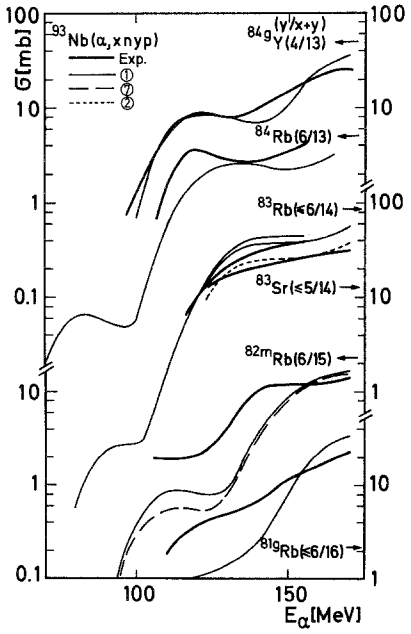

Fig. 12. ^{93}Nb(^{4}He, $xn\,yp$) excitation function in comparison with INDEX model predictions. Same notation as in Fig. 8

the code does not account for PE α-emission. In the measured yields for ^{90,89m,88}Nb and ^{89,88,86}Zr (Figs. 10, 11) this process leads to a typical filling of the valley between the first maximum due to α-emission and the following rather flat plateau where nucleon emission dominates. For the residual nuclei ^{88,87,86,85,84}Y as well as for ^{85m,83}Sr the emission of two α-particles is possible (Figs. 10–12). The first α-bumps clearly show up in the measurements as well as in the predictions down to ^{84}Y and ^{85m}Sr. The isotopes of rubidium, ^{84,83,82m}Rb, can be reached by the emission of three α-particles. According to our calculations, however, the first α-bump is very weak. In fact, it has not been observed except for a slight indication in the ^{82m}Rb yield curve (Fig. 12).

Generally, the curves due to set (1) somewhat better account for the mentioned α-bumps in the excitation functions. However, they mostly overpredict the measured yields in the region of multi-nucleon emission. Here, set (2) with $n_0=5$ displays a somewhat better agreement with the data. The rise and fall of the excitation functions is, on the whole, quite well reproduced by the s-wave option together with the soft pairing in the level density. The drawback of the s-wave approximation clearly shows up for the case of maximum nucleon emission leading to the isotopes of ^{84,82m,81g}Rb: the large amount of frozen-in rotational energy cannot be regained by the emission of the more energetic charged particles so that the predicted rise of the excitation functions is shifted more and more to higher energies.

5. Conclusions

In its present form, the EXCLUSIVE INDEX code, in connection with the slightly modified particle evaporation code OVERLAID ALICE [10], is able to predict residual nucleus yields up to 200 MeV excitation energy [6, 14]. We have compared the model predictions with a large variety of excitation functions from p, d, ^{3}He and ^{4}He induced reactions in the mass range $A=89$–209 up to 170 MeV bombarding energy. Also residual nucleus yields from stopped π^--induced reactions on ^{197}Au and ^{209}Bi are well reproduced [30].

With regard to the global set of CN input parameters the predictions agree remarkably well with the experimental data except where PE α-emission, which is not included in the INDEX model, gets stronger than the emission of four separate nucleons. Larger deviations also occur in case of strong stripping or breakup processes, especially at lower bombarding energies of complex projectiles [25]. While part of the projectile stays outside the target as a mere spectator one or more nucleons are captured into s.p. states [29]. In the language of PE decay, the typical spectra due to these processes are roughly reproduced by smaller initial degrees of freedom than found for the total equilibration of target and projectile.

For smaller numbers of emitted nucleons (say $x+y\leqq 8$) it was found that the s-wave approximation better describes the onset of excitation functions while for a larger number of emitted nucleons the simple Weisskopf-Ewing approach is more favourable. The

Table 2. Global set of parameters used in the analysis of excitation functions

Projectile	Target	$n_0(p_\nu, p_\pi)$	E_F (MeV)	k_{MFP}	$x+y$
p	^{89}Y	2.5(0.66, 1.34)	20	4[a]	$\geqq 1$
	^{209}Bi	2.5(0.75, 1.25)	20	4[a]	$\geqq 1$
d	^{181}Ta	4(1.5, 1.5)	20	4[a]	$\geqq 1$
^3He	^{197}Au	5(1.6, 2.4)	20	2	$\geqq 1$
^4He	^{93}Nb, ^{181}Ta	5(2.5, 2.5)	20(40)	2(1)	$\leqq 2$, $\geqq 8$
		6(2.5, 2.5)	20(40)	2(1)	>2

[a] Inclusion of the finite hole depth in the calculation of exciton densities with $n_0 = 3(p)$ or $4(d)$ would result in $k_{MFP} \approx 2$ (see text)

PE input parameters providing the best global fits are listed in Table 2. The results confirm the thumb rule $n_0 \approx A_{proj.} + 2$. As though excitation functions for a large number of removed nucleons ($x+y \geqq 8$) are not so sensitive to the choice of n_0 preequilibrium multiparticle emission still plays a visible role. Calculations with only one PE nucleon cannot well reproduce the rather slow decline or practically constant yield in the high energy part of these excitation functions (e.g. curves for $A = 90$–85 in Figs. 10 and 11). We hold this feature as important as the possibly more striking result that the computed (d, $2p$), and (^4He, $2p$) excitation functions in Figs. 5 and 9 do quite well agree with the experiment regarding shapes and absolute yields. Here, the predictions for one PE particle out are too low by several orders of magnitude (cf. [31]).

With respect to the detailed study of the $^4He + ^{93}Nb$ reaction the INDEX model describes the data as well as the quite sophisticated analysis of Gadioli et al. [28] where four contributing processes are considered: inelastic ^4He scattering, binary fragmentation of the projectile, and dissolution of ^4He in the field of the target nucleus, all leading to $n_0 = 4$ starting configurations, as well as ^4He-nucleon collisions leading to $n_0 = 6$. Indeed, our analyses agree with the presence of more direct reactions like two- or three-particle stripping [29] that contribute to few-nucleon emission at lower energies, and require $n_0 = 5$ for $x+y \leqq 2$. Though one notes the neglect of PE α-emission in our model the features of most excitation functions are well explained PE and CN nucleon emission alone, and with less assumptions. We also point out that our analysis is consistent with a mean-free-path multiplier $k_{MFP} = 2 (E_F = 20$ MeV) while the EXCITON model fits require twice that value [21, 28] using the same Fermi energy. This fact corroborates similar conclusions we gained from the analysis of spectra [5] and yields of other light-ion induced reactions. The noted discrepancy is related to intrinsic statistical differences in both models [2, 32, 33]. Roughly speaking, in the INDEX model only the life-time of particles is important while in the EXCITON model the interaction of holes counts as well. Hence, for getting the same particle emission probability as in the model of independently interacting excitons, the resulting faster nuclear equilibration has to be compensated by doubling k_{MFP}.

Concerning the absolute value of the mean free path of nucleons in nuclear matter the present analyses and others of this kind [31, 33–35] can hardly give a unique answer [36]. In the frame of the simplified Fermi gas model they may provide an effective mean value, at best. Firstly, because the interaction length of nucleons in finite nuclei is not a well defined quantity, in view of potentials and densities rapidly changing with the impact parameter of the projectile [36, 37]. Secondly, our analysis shows that parameter sets with a constant product of $E_F \times k_{MFP} \approx 40$ MeV are practically equivalent for light ion induced reactions. According to Kikuchi and Kawai [38], the values $k_{MFP} = 2$ and $E_F = 20$ MeV lead to a rising mean free path of 7–12 fm for 30–200 MeV proton energy while for $k_{MFP} = 1$ and $E_F = 40$ MeV the mean free path drops from about 3.6 to 2.6 fm! For $E_F = 30$ MeV and $k_{MFP} = 1.33$ one would get a mean free path of 4–5 fm that would nicely agree with results from nuclear matter calculations by Negele et al. [39] and with those from analyses of the imaginary part of the optical potential [33, 39]. Regarding PE investigations the ambiguity in E_F and k_{MFP} would be solved if, as suggested in [5], a more refined analysis of appropriate nucleon spectra were able to deduce the average depth of the nuclear potential.

Concluding we think the very value of the present approach lies in its simple ansatz which is carried through by help of an admittedly intricate statistics. For reactions where the whole projectile fuses with the target and initiates PE and CN equilibration cascades the present EXCLUSIVE INDEX model code quite well predicts the complex partition of the reaction flux into the many residual nuclei. The code can easily be extented to energies beyond 200 MeV. Then however, in order to be meaningful, three particle emission from up to three PE stages has to be included together with PE emission of light clusters – a task that requires new, quick and powerful approximations.

Appendix

Average Angular Momentum Decoupling in Evaporation Cascades

In the computational treatment of long evaporation cascades the full book-keeping of angular momentum

effects by Hauser-Feshbach type calculations [16] is rather prohibitive since large energy-spin matrices have to be populated and depopulated when going from one nucleus to the other. In addition, a large set of transmission coefficients $T_L(E)$ has to be used for each ejectile of a particular energy instead of the *one* inverse cross section entering the simple Weisskopf-Ewing approach [15]. On the other hand angular momentum effects do play an important role. In the mid-sixties several practical compromises have been discussed by T.D. Thomas and others [7], one being the *s*-wave approximation mentioned above. Keeping the notations of Sect. 3.2. we want to outline a more general scheme which allows to treat on average the angular momentum decoupling in even long evaporation chains. We start from the rate expression of T.D. Thomas [7, (3.1)] for populating a residual nucleus of excitation energy U' and total spin J' by emission of particle x of kinetic energy ε_x and spin s_x from the preceding compound nucleus of energy U and total spin J with $\mathbf{J}'$ and $\mathbf{s}_x$ coupling to the channel spin $\mathbf{S}$. The transmission coefficients are assumed to depend only on the orbital angular momentum L but not on the coupling of $\mathbf{s}_x$, $\mathbf{J}'$ and $\mathbf{J}$ to $\mathbf{L}$. Summing over all final spins J' yields the total rate expression

$$R_x(U,J,U')\,\mathrm{d}\varepsilon_x = \sum_{J'=0}^{\infty} h^{-1}\Omega(U',J')/\Omega(U,J) \sum_{S=|J'-s_x|}^{J'+s_x} \sum_{L=|J-S|}^{J+S} T_L(\varepsilon_x)\,\mathrm{d}\varepsilon_x. \tag{A1}$$

As in Sect. 3.2 we use a level density form according to [14]:

$$\Omega(U,J) = \text{const.}(2J+1)\,\rho(U,J) \tag{A2a}$$

The reduced level density $\rho(U,J)$ is given by

$$\rho(U,J) = (U-E_{\mathrm{rot}}(J)+\Delta)^{-2}\exp\{2[a(U-E_{\mathrm{rot}}(J)+\Delta)]^{1/2}\} \tag{A2b}$$

The rotational energy is determined by

$$E_{\mathrm{rot}}(J) = J(J+1)\hbar^2/2\theta \tag{A3}$$

where θ is the moment of inertia.

The main point of the present approach is that the residual nucleus level density is assumed to be strictly proportional to $(2J'+1)$:

$$\Omega(U',J') = \text{const.}(2J'+1)\,\rho_{\mathrm{eff}}(U', J'_{\mathrm{eff}}(x,\varepsilon_x,J)) \tag{A4}$$

i.e. the rotational energy of the residual nucleus is approximated by a constant, $E_{\mathrm{rot}}(J'_{\mathrm{eff}}(x,\varepsilon_x,J))$. The effective average spin may be suitably chosen for each value of the total spin J of the parent CN nucleus. It may also depend on the energy ε_x of particle x. Reversing the order of summation in (A 1) and leaving out constant terms for fixed total spin J one gets

$$\begin{aligned}&\sum_{J'=0}^{\infty}(2J'+1)\sum_{S=|J'-s_x|}^{J'+s_x}\sum_{L=|J-S|}^{J+S} T_L(\varepsilon_x)\\ &=(2J+1)(2s_x+1)\sum_{L=0}^{\infty}(2L+1)\,T_L(\varepsilon_x)\\ &=(2J+1)(2s_x+1)\,2\mu_X\,\varepsilon_X\,\sigma_{\mathrm{inv}}(\varepsilon_x)/(\pi\hbar^2)\end{aligned} \tag{A6}$$

applying the usual definition for inverse cross sections. This leads to the final result

$$R_x(U,J,U')\,\mathrm{d}\varepsilon_x = \text{const.}(2s_x+1)\,\mu_X\,\varepsilon_X\,\sigma_{\mathrm{inv}}(\varepsilon_x)\cdot\rho_{\mathrm{eff}}(U', J'_{\mathrm{eff}}(x,\varepsilon_x,J))/\rho(U,J)\,\mathrm{d}\varepsilon_x. \tag{A7}$$

The probability $P_x(U,J,U')\,\mathrm{d}\varepsilon_x$ to populate a specific energy bin of the residual nucleus, $U'+\mathrm{d}\varepsilon_x$ is given by

$$P_x(U,J,U')\,\mathrm{d}\varepsilon_x = R_x(U,J,U')\,\mathrm{d}\varepsilon_x \Big/ \sum_{x'}\int_{\varepsilon_{x'}=0}^{\varepsilon_{x'}(\max)} R_{x'}(U,J,U')\,\mathrm{d}\varepsilon_{x'}. \tag{A8}$$

In this expression the parent CN level density expression $\rho(U,J)$ for spin J drops out. In evaporation cascades the effective average spin $J'_{\mathrm{eff}}(x,\varepsilon_x,J)$ of a nucleus gets the starting spin "J" for the next transition. Many approaches, also such dependent on specific particle energies seem to be feasible.

One simple but quite effective approach would be decoupling prefixed amounts of angular momentum for each ejectile in a consistent manner, e.g. $\Delta J = J - J'_{\mathrm{eff}}(x,\varepsilon_x,J) = 2$ for neutrons, $\Delta J = 3$ for protons, $\Delta J = 5$ for deuterons and $\Delta J = 10$ for alphas, an option that has been already introduced by Blann [10]. Here, for each value of the initial partial wave angular momentum J, the spin $J'_{\mathrm{eff}}(J,Z',N')$ does only depend on the number of removed nucleons but not on the individual path the nucleus $A'(Z',N')$ is reached by *n*-, *p*-, *d*- or α-emission cascades.

On the other hand, putting $\Delta J = J - J'_{\mathrm{eff}}(x,\varepsilon_x,J) = 0$ automatically leads to the usual *s*-wave approximation for evaporation cascades. There, the rotational energies may be subtracted from the beginning if all residual nuclei do possess the same moment of inertia. However, if fission is important separate CN calculations have to be made for each incoming partial wave because fission probabilities, and hence reaction thresholds vary with the entrance channel angular momentum. Also the changing moment of inertia in CN decay chain nuclei then has to be observed

for a proper energy book-keeping. In order to account for these effects in the code INDEX [6] we have considerably altered the nesting of routines as compared to the OVERLAID ALICE code [10].

References

1. Ernst, J., Friedland, W., Stockhorst, H.: Z. Phys. A – Atomic Nuclei **328**, 333 (1987)
2. Ernst, J., Rama Rao, J.: Z. Phys. A – Atoms and Nuclei **281**, 129 (1977)
3. Stockhorst, H., Friedland, W., Ernst, J.: Proceedings of the 3rd International Conference on Nuclear Reaction Mechanisms, Varenna, June 14–19, 1982, Gadioli, E. (ed.), p. 119; Friedland, W.: Dissertation, University of Bonn, 1984 (unpublished)
4. Ernst, J., Friedland, W., Stockhorst, H.: Laborbericht, Institut für Strahlen- und Kernphysik, Universität Bonn, 1987 (unpublished)
5. Ernst, J., Friedland, W., Stockhorst, H.: Z. Phys. A – Atomic Nuclei **328**, 445 (1987)
6. Friedland, W., Stockhorst, H., Ernst, J.: Computer code INDEX, 1984 (unpublished), the code is available on request
7. Thomas, T.D.: Nucl. Phys. **53**, 558 (1964); Esterlund, R.A., Pate, B.D.: Nucl. Phys. **69**, 401 (1965); M. Blann, G. Merkel: Phys. Rev. **137**, B367 (1965)
8. Metropolis, N., Bivins, R., Storm, M., Miller, J.M., Friedlander, G., Turkevich, A.: Phys. Rev. **110**, 204 (1958)
9. Bissem, H.H., George, R., Scobel, W., Ernst, J., Kaba, M., Rama Rao, J., Strohe, H.: Phys. Rev. C**22**, 1468 (1980)
10. Blann, M.: OVERLAID ALICE, US ERDA Report COO-3494-29, 1976
11. Thomas, T.D.: Phys. Rev. **116**, 703 (1959)
12. Wapstra, A.H. Gove, N.B.: Nucl. Data Tables **9**, 267 (1971)
13. Wapstra, A.H., Bos, K.: At. Data Nucl. Data Tables **19**, 175 (1977)
14. Bohr, A., Mottelson, B.: Nuclear structure, Vol. 1. New York, Amsterdam: W.A. Benjamin
15. Weisskopf, V., Ewing, D. H.: Phys. Rev. **57**, 472 (1940)
16. Hauser, W., Feshbach, H.: Phys. Rev. **87**, 336 (1952)
17. Cohen, S., Plasil, F., Swiatecki, W.J.: Ann. Phys. **82**, 557 (1974); LDM moments of inertia are incorporated in [10]
18. Ernst, J., Ibowski, R., Klampfl, H., Machner, H., Mayer-Kuckuk, T., Schanz, R.: Z. Phys. A – Atoms and Nuclei **308**, 301 (1982); Hermes, F., Jasper, E.W., Kurz, H.E., Mayer-Kuckuk, T.: Nucl. Phys. A**228**, 165 (1974)
19. Saha, G.B. Porile, N.T. Yaffe, L.: Phys. Rev. **144**, 962 (1966)
20. Le Beyec, Y., Lefort, M.: Nucl. Phys. **99**, 131 (1967)
21. Gadioli, E., Gadioli-Erba, E., Hogan, J.J.: Phys. Rev. C**16**, 1404 (1977)
22. Jahn, P., Probst, H.J., Djaloeis, A., Davidson, W.F., Mayer Böricke, C.: Nucl. Phys. A**209**, 333 (1973); Michel, R., Galas, M.: Int. J. Appl. Radiat. Isot., **34**, 1325 (1983); Rama Rao, J., Ernst, J., Machner, H.: Nucl. Phys. A**448**, 365 (1986)
23. Bisplinghoff, J., Ernst, J., Mayer-Kuckuk, T., Jahn, T., Mayer-Böricke, C.: Nucl. Phys. A**228**, 180 (1974)
24. Rama Rao, J., Ernst, J., Machner, H.: Nucl. Phys. A**448**, 365 (1986)
25. Baur, G., Rösel, F., Trautmann, D., Shyam, R.: Phys. Rep. **111**, 333 (1984)
26. Bousshid, O.: KFA Report, Jül. Spez.-98, Jülich 1981 (unpublished)
27. Marten, M., Schüring, A., Scobel, W., Probst, H.J.: Z. Phys. A – Atomic Nuclei **322**, 93 (1985)
28. Gadioli, E., Gadioli-Erba, E., Hogan, J.J., Jacak, J.V.: Phys. Rev. C**29**, 76 (1984)
29. Jahn, R., Wienands, U., Wenzel, D., Neumann-Cosel, P. v.: Phys. Lett. **150**B, 331 (1985)
30. Stockhorst, H., Ernst, J.: Proceedings of the International Symposium on Collective Phenomena in Nuclear and Subnuclear Long Range Interactions in Nuclei, Bad Honnef, May 4–7, 1987, P. David, (ed.), p. 336 Lecture Notes in Physics. Berlin, Heidelberg, New York: Springer 1988
31. Blann, M., Vonach, H.K.: Phys. Rev. C**28**, 1475 (1983)
32. Bisplinghoff, J: Phys. Rev. C**3**, 1569 (1986)
33. Blann, M.: Ann. Rev. Nucl. Sci. **25**, 123 (1974)
34. Machner, H.: Phys. Rep. **127**, 309 (1985)
35. Gadioli, E., Gadioli-Erba, E.: Nucl. Instrum. Methods **146**, 265 (1977); see also [21]
36. Ernst, J., Friedland, W., Stockhorst, H.: In: Publishing House of the Bulgarian Academy of Sciences, Sofia 1984, Proceedings of the 6th International School on Nuclear Physics, Neutron Physics and Nuclear Energy, Varna/Bulgaria, September 12–21, 1983, p. 247
37. Di Giacomo, N.J., De Vries, R.M., Peng, J.C.: Phys. Rev. Lett. **45**, 527 (1980); Di Giacomo, N.J., De Vries, R.M.: J. Phys. G: Nucl. Phys. **7**, L51 (1981)
38. Kikuchi, K., Kawai, M.: Nuclear matter and nuclear reactions. Amsterdam: North Holland 1968
39. Negele, J.W.: Comments Nucl. Part. Phys. **12**, 1 (1983); Negele, J.W., Yazaki, K.: Phys. Rev. Lett. **47**, 71 (1981)

J. Ernst, H. Stockhorst
Institut für Strahlen- und Kernphysik
Universität Bonn
Nussallee 14–16
D-5300 Bonn 1
Federal Republic of Germany

W. Friedland
Gesellschaft für Strahlen- und Umweltforschung mbH München
Ingolstädter Landstrasse 1
D-8042 Neuherberg
Federal Republic of Germany